THE JOURNAL OF CHEMICAL PHYSICS **143**, 154109 (2015)

Driven diffusion against electrostatic or effective energy barrier across α-hemolysin

Patrizio Ansalone,[1,a)] Mauro Chinappi,[2,a)] Lamberto Rondoni,[3] and Fabio Cecconi[4,b)]
[1]*Istituto Nazionale di Ricerca Metrologica, Strada delle Cacce 91, Torino, IT-10135, Italy*
[2]*Center for Life Nano Science@Sapienza, Istituto Italiano di Tecnologia, Via Regina Elena 291, 00161 Roma, Italy*
[3]*Scienze Matematiche, Politecnico di Torino Corso Duca degli Abruzzi 24, Torino, IT-10129, Italy and INFN, Sez. di Torino, Via P. Giuria 1, Torino IT-10125, Italy*
[4]*CNR-Istituto dei Sistemi Complessi UoS "Sapienza," Via dei Taurini 19, 00185 Roma, Italy*

(Received 18 June 2015; accepted 30 September 2015; published online 21 October 2015)

We analyze the translocation of a charged particle across an α-Hemolysin (αHL) pore in the framework of a driven diffusion over an extended energy barrier generated by the electrical charges of the αHL. A one-dimensional electrostatic potential is extracted from the full 3D solution of the *Poisson*'s equation. We characterize the particle transport under the action of a constant forcing by studying the statistics of the translocation time. We derive an analytical expression of translocation time average that compares well with the results from Brownian dynamic simulations of driven particles over the electrostatic potential. Moreover, we show that the translocation time distributions can be perfectly described by a simple theory which replaces the true barrier by an equivalent structureless square barrier. Remarkably, our approach maintains its accuracy also for low-applied voltage regimes where the usual inverse-Gaussian approximation fails. Finally, we discuss how the comparison between the simulated time distributions and their theoretical prediction results to be greatly simplified when using the notion of the empirical Laplace transform technique. © *2015 AIP Publishing LLC.* [http://dx.doi.org/10.1063/1.4933012]

I. INTRODUCTION

Theoretical and computational approaches to driven or spontaneous migration of molecules through a biological pore are often based on idealized models whereby pores are represented as passive channels imposing a spatial confinement[1–5] that basically results into the presence of an entropic barrier.[6,7] While this raw geometrical picture may be appropriate to investigate a general principle of the transport of neutral species across solid state nano-channels, it turns out to be drastic for biological pores whose chemical composition is known to affect the translocation mechanism of charged molecules. Both experiments and simulations have, indeed, revealed that pore charges strongly influence the translocation under the effect of driving forces.[8–13] Therefore, the electrostatic interaction between a pore and the charged molecules cannot be neglected in reasonably realistic phenomenological models of translocation.

From a theoretical perspective, the passage of molecules through a nanopore can be viewed as overcoming a free-energy barrier determined by the physical properties of the pore and molecule system. This problem is commonly tackled as a driven-diffusion process in the presence of a given free-energy landscape,[14–18] which, under suitable approximations, leads to solving a one-dimensional driven diffusion *Smoluchowski* equation,[19] with appropriate initial and boundary conditions.

The main purpose of this paper is to analyze the driven diffusion of a charged particle in the presence of realistic electrostatic potential. As a relevant example, we selected the α-Hemolysin (αHL) pore, a biological pore widely employed in nanopore technology[20–28] that spontaneously self assembles into a heptameric channel that inserts itself into a lipid bilayer. First, we compute numerically the 3D electrostatic potential generated by the αHL, then we interpolate the effective one-dimensional profile along the pore channel. In the Smoluchowski driven-diffusion picture, such a 1D-potential corresponds to an energy barrier that a charged particle has to overcome in order to cross the pore, with the simplified assumption that the translocating particle does not perturb the charge distribution and does not affect the electrostatics of the αHL. In that context, the translocation of a charged monomer is assimilated to a first passage process of a Brownian charged particle entering the pore in one side and reaching the opposite one. The statistical properties of the translocation are then obtained either by direct numerical integration of the Langevin equation or via the computational or analytical solution of the Smoluchowski equation.[19]

In this study, we derive an analytical expression for the average passage-time as a function of the external load for generic 1D barrier. In addition, for the specific case of a square barrier, we find a closed expression for the Laplace transform of the passage time distribution. Interestingly, the distributions numerically obtained, with the 1D potential, are well matched by the theoretical one with an equivalent square barrier. As a final remark, our results suggest that the fitting

a)P. Ansalone and M. Chinappi contributed equally to this work.
b)Electronic mail: fabio.cecconi@roma1.infn.it

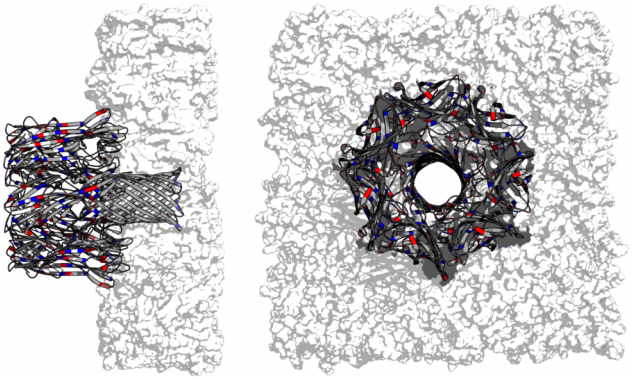

FIG. 1. The mushroom-shaped protein αHL consists of a vestibule with a diameter ≈46 Å at its widest section and 50 Å in length. The vistibule is linked to a β-barrel transmembrane whose diameter is ≈25 Å and 50 Å in length. The interface between the vestibule and the β-barrel domains shows a bottleneck; in this region, the pore is ≈14 Å wide at its narrowest point.

procedure of theoretical first passage-time distributions to numerical or experimental data can be conveniently carried out via the empirical Laplace technique.[29]

The present paper is organized as follows. Section II describes the electrostatic model adopted in an ideal free salt environment. In Section III, we briefly introduce the *Smoluchowski* description for driven diffusion, we derive the analytical solution for the average passage time for a generic free-energy profile, and we obtain the Laplace transform of the translocation time distribution for the square barrier. Numerical results for the first passage time distributions are reported and discussed in Section IV.

II. ELECTROSTATIC POTENTIAL BARRIER

This section presents the computation of the electrostatic potential inside and outside the (αHL) pore in a free salt medium. The αHL length is approximatively $L = 100$ Å, and it is subdivided in several regions, Figure 1. The β-barrel region (it is embedded in the lipid membrane) has a diameter of ≃20 Å (based on backbone), the vestibule is 46 Å in diameter, and the narrowest section, located between the vestibule and the β-barrel, is approximatively 14 Å wide. The pore is embedded in a lipid membrane approximatively of 40 Å thickness. In this study, αHL is aligned along the x-axis. The *Laplace* and *Poisson* equations are numerically solved in order to calculate the electrostatic potential $V(\mathbf{r})$,

$$\begin{cases} \nabla^2 V = 0 & \text{in } \Omega_{H_2O}, \Omega_m \subset \mathbb{R}^3 \\ \nabla^2 V = -\sum_{i=1}^{N_q} \frac{q_i}{\varepsilon_p \varepsilon_0} \delta(\mathbf{r} - \mathbf{r}_i) & \text{in } \Omega_p \subset \mathbb{R}^3 \end{cases} . \quad (1)$$

Here, Ω_{H_2O} is the solvent region occupied by the water, Ω_m is the lipid membrane region, and Ω_p is the region occupied by αHL, while ε_0 and ε_p are the vacuum and pore dielectric constants, respectively. The N_q point charges q_i in Eq. (1) are obtained from the Protein Data Bank (PDB) structure of αHL (pdb code: 7AHL),[20] and the protonation state for residues is determined at pH 7.0 employing the PDB2PQR pipeline[30] and the AMBER99 force field.[31] Briefly, in order to simulate the entire system, we carried out a dummy calculation with APBS-FETK software libraries[32] to create 3D dielectric environment and the geometry of a previously equilibrated lipid membrane. The dielectric constant of each region of the structure is homogeneous, and the values are chosen as follows: in Ω_{H_2O}, the standard relative dielectric is $\varepsilon_{H_2O} = 78.54$. For the pore, $\varepsilon_p = 4$ and $\varepsilon_m = 2$ for the lipid membrane region. The system of equations is solved using the APBS-FETK.[32–34] The simulation is run assuming a bounding box equal to 321 Å × 321 Å × 321 Å with a fine grid of 1 grid nodes/Å. The Eq. (1) is numerically solved enforcing Dirichlet boundary condition and continuity of the potential and normal electric displacement across the interfaces among solvent, lipid membrane, and αHL regions. To obtain a 1D profile of the electrostatic potential as a function of the x-coordinate from the 3D electrostatic potential, we use the following procedure. First, we chose nine directions of sight, labelled by ω_i in Figure 2, at a distance of 1 Å from the x-axis of the pore, then we interpolate the electrostatic potential for each one of them. Since the potential appears to be only slightly dependent on the position ω_i, inside the pore, we take the average as electrostatic barrier experienced by a charged particle translocating through the pore (inset of Figure 2). Finally, the average electrostatic potential $\bar{U}(x)$ is fitted with a multi-Gaussian function. Figure 2 shows the behavior of the electrostatic potentials along the x-axis of the αHL pore. The peak in the electrostatic potential

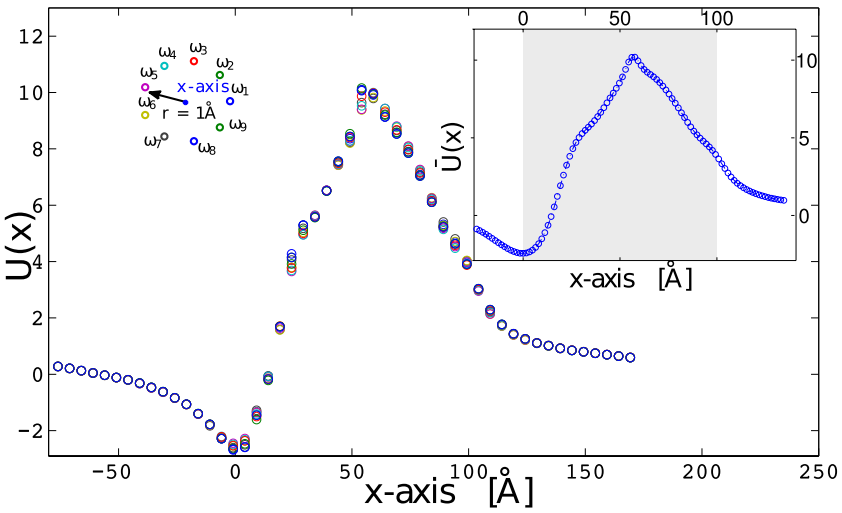

FIG. 2. Dimensionless unit $k_B T e^{-1}$ of the electrostatic potential along the x-axis of the αHL. The behavior of the electrostatic potential is plotted taking into account nine different lines of sight, each one at a 1 Å distance from the x-axis. The highest value in the electrostatic potential is located approximately 40 Å from the origin of the reference frame (i.e., the cap of the αHL). It corresponds to the location of a group of Lys[147] residues. The average of the electrostatic potential is shown in the inset. The grey shaded area corresponds to the pore region.

is mostly localized between the seven Lys[147], and these residues form a ring around the narrowest part of the β-barrel region. In contrast, the electrostatic effects arising from Asp[127] and Asp[128] (negatively charged) are partially compensated by Lys[131] (positively charged), and these residues flatten the peak of the electrostatic potential at the end of the β-barrel region ($x \approx 100$ Å). These results are in agreement with the previous studies.[35]

III. SMOLUCHOWSKI DRIVEN DIFFUSION

Here, we describe the one-dimensional *Smoluchowski* equation for a positively charged particle q driven by a constant electrical field E_x along the x-axis, $F = qE_x$ in the presence of a generic energy barrier. The probability $P(x,t)$ for a particle to be in the position x at time t satisfies the conservation equation

$$\frac{\partial P}{\partial t} = -\frac{\partial J}{\partial x}, \tag{2}$$

where $J(x,t)$ is the flux of probability density. In the present case, Eq. (2) takes the form

$$J(x,t) = -D\frac{\partial P}{\partial x} - \mu P\frac{\partial \bar{U}(x)}{\partial x} + \mu PF, \tag{3}$$

where μ and $D = \mu k_B T$ are the particle mobility and diffusion coefficient, respectively, with T the temperature and k_B the Boltzmann constant. The function $\bar{U}(x)$ denotes the barrier profile due to the pore as defined in the previous section and F is the applied bias electric force acting over the whole domain $[-\infty, L]$. The pore occupies the region $x \in (0, L)$. Particles are emitted at the pore entrance, $x = 0$, at time $t = 0$, and are later adsorbed at $x = L$, which implies the boundary condition $P(L,t) = 0$, see Fig. 3. In the following, unless differently specified, we use the natural dimensionless variables: $\tilde{x} = L^{-1}x, \tilde{t} = DL^{-2}t$, $\tilde{F} = LF/k_BT$. In these coordinates, the pore region $[0, L]$ is rescaled to the interval $[0, 1]$. For sake of notation simplicity, we omit the tilde, so that the dimensionless Smoluchowski equation reads

$$\frac{\partial P}{\partial t} = \frac{\partial}{\partial x}\left[\frac{\partial P}{\partial x} + P\frac{\partial \bar{U}(x)}{\partial x} - FP\right]. \tag{4}$$

Integrating the solution $P(x,t)$ of Eq. (4), we obtain the probability $S(t)$ that at time t the particle has not yet translocated

$$S(t) = \int_{-\infty}^{1} P(x,t)dx. \tag{5}$$

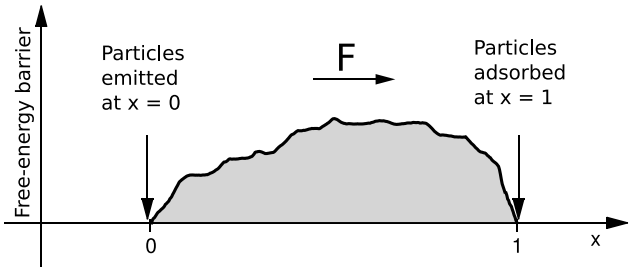

FIG. 3. Sketch of the 1-D driven-diffusion model. Particles are emitted at the pore entrance $x = 0$ and are adsorbed at the pore exit ($x = 1$). Translocation requires the overcoming of the free-energy barrier with the help of an external force F acting along the x direction.

This is also called the survival probability, as in our model, it is the probability that the particle has not been absorbed at $x = 1$. Accordingly, the probability to be absorbed, i.e., to exit the pore after the time t, is $P_{\text{out}}(t) = 1 - S(t)$. Therefore, the distribution of first passage times $\psi(t)$ is simply obtained as

$$\psi(t) = \frac{dP_{\text{out}}(t)}{dt} = -\frac{dS(t)}{dt}. \tag{6}$$

Using Smoluchowski equation (4), we can express $\psi(t)$ in terms of the probability current at the absorbing boundary

$$\psi(t) = J(1,t) = -\frac{\partial P}{\partial x}\Big|_1 - P(1,t)\,\frac{\partial \bar{U}(x)}{\partial x}\Big|_1 + FP(1,t), \tag{7}$$

thus the probability current, through the solution of Eq. (4), determines $\psi(t)$. The knowledge of $\psi(t)$ allows us to derive all moments of the distribution and, in particular, the average translocation time,

$$\tau = \int_0^\infty dt\, t\, \psi(t) = \int_{-\infty}^{1} dx \int_0^\infty dt P(x,t), \tag{8}$$

where the second equality follows from Eqs. (6), (5), and from an integration by parts. Appendix A shows that, for a generic barrier of shape $\bar{U}(x)$, the Smoluchowski equation in the domain $[-\infty, 1]$ with initial condition $P(x,0) = \delta(x)$ provides the expression

$$\tau = \frac{M_+(F)}{F} + M_0(F), \tag{9}$$

where the functions $M_+(F)$ and $M_0(F)$ are given by

$$\begin{aligned} M_+(F) &= \int_0^1 dx\, e^{G(x)}, \\ M_0(F) &= \int_0^1 dx\, e^{-G(x)} \int_x^1 dy\, e^{G(y)}, \end{aligned} \tag{10}$$

with $G(x) = \bar{U}(x) - Fx$. Interestingly, in the limit $F \to 0$, the second term of Eq. (9) becomes negligible and

$$\tau \simeq \frac{M_+(0)}{F}. \tag{11}$$

As we will see in the following, this allows an equivalent square barrier to be defined with height

$$\phi = \log M_+(0). \tag{12}$$

While the explicit value of τ can be obtained numerically, at least, computing the relevant integrals, the explicit expression of $\psi(t)$ for an arbitrary barrier cannot be given. Indeed, Eq. (7) requires the full solution of (4) which, in general, cannot be worked out analytically. Consequently, one must either resort to direct numerical simulations or introduce simplifying approximations.

A simple but meaningful approximation amounts to replacing the actual potential barrier with a square profile which allows us to derive a closed analytical form for the Laplace transform $\hat{\psi}(s)$ of $\psi(t)$, and which appears to be "equivalent" to the real barrier for calculations of our concern. Indeed, as detailed in Appendix A, the Laplace transform of the Smoluchowski equation yields the result

$$\hat{\psi}_\phi(s) = \frac{2e^{F/2}A(F,s)}{[2e^\phi A(F,s) + F(1-e^\phi)]\sinh[A(F,s)] + 2A(F,s)\cosh[A(F,s)]}, \tag{13}$$

where $2A(F,s) = \sqrt{F^2+4s}$, and ϕ is the barrier height, i.e., $\bar{U}(x) = \phi$ for $x \in [0,1]$ and $\bar{U}(x) = 0$, $x \in [-\infty, 0]$. As we shall see in Section IV, the expression of $\hat{\psi}(s)$ is very useful in the analysis of the empirical Laplace transform[29] of the translocation times obtained from direct simulations, even without the explicit inversion. Eq. (13) reduces to the well known *Inverse Gaussian* (IG) distribution obtained in the vanishing barrier limit, $\phi = 0$,

$$\hat{\psi}_{IG}(s) = \exp\left\{\frac{1}{2}\left(F - \sqrt{F^2+4s}\right)\right\}, \tag{14}$$

which can be easily inverted to give

$$\psi_{IG}(t) = \frac{1}{\sqrt{4\pi t^3}}\exp\left\{-\frac{(1-Ft)^2}{4t}\right\}, \tag{15}$$

customarily considered a useful guide to interpret data of voltage-driven translocation experiments in high-voltage regimes.[36] At the end of Appendix B, we show that, though the inversion of Eq. (13) leads to a quite involved expression, the large-time behaviour of the arrival time probability distribution function (PdF) can be easily worked out via a saddle-point method (see Eq. (B12)) and reads

$$\psi_\phi(t) \sim \exp\left\{-\frac{F^2e^\phi}{(1+e^\phi)^2}\,t\right\}. \tag{16}$$

Interestingly, the exponential decay rate is controlled by the height of the equivalent barrier and, when $\phi \to 0$, it is consistent with the inverse Gaussian behaviour $\exp(-F^2t/4)$.

Using the relation between the derivatives of the Laplace transform calculated at $s = 0$ with the momenta of the function, $(-1)^n\hat{\psi}^{(n)}(0) = \int_0^\infty dt\, t^n\psi(t)$, where (n) indicates the n-th derivative, we can obtain all the momenta of ψ, in particular, the average residence time reads

$$\tau = \frac{F + (e^\phi - 1)(1-e^{-F})}{F^2}. \tag{17}$$

Notice that Eq. (17) can be also directly derived by Eq. (9). Interestingly, in the limit of $F \to 0$, (17) reduces to

$$\tau = \frac{e^\phi}{F}, \tag{18}$$

i.e., again a $1/F$ behavior as in the $F \to \infty$ limit. By comparison of Eqs. (18) and (11), it results that, in the limit $F \to 0$, any barrier can be described by an equivalent square barrier, the correspondence being set via the following relation:

$$\exp(\phi) = M_+(0) = \int_0^1 dx\, e^{U(x)}. \tag{19}$$

IV. NUMERICAL RESULTS

The electrostatic barrier derived in Section II is used to study numerically the translocation of a positive unit charge across the αHL under the action of a constant electric field E. We generate a continuous version of 1D average electrostatic potential by a multi-Gaussian fit,

$$\bar{U}(x) = \sum_{k=0}^{7} \bar{U}_k \exp\left[-\left(\frac{x-x_k}{c_k}\right)^2\right]. \tag{20}$$

The set of coefficients is reported in Table I. The dynamics of the charged particle is described by the overdamped Langevin equation

$$\dot{x} = F - \frac{\partial \bar{U}(x)}{\partial x} + \sqrt{2}\eta(t), \tag{21}$$

with $\eta(t)$ a Gaussian noise, with $\langle\eta(t)\rangle = 0$ and $\langle\eta(t)\eta(t')\rangle = \delta(t-t')$. After ensemble averaging, this Langevin approach is equivalent to Smoluchowski formulation (4).[19] In Langevin formulation (21), we assume the friction exerted by the solvent large enough to overwhelm the inertial terms (overdamped regime). We integrated equation (21) numerically via a second order stochastic Runge-Kutta algorithm,[37] for an ensemble of $M = 10^5$ independent particles emitted at the pore entrance ($x = 0$) at $t = 0$ and adsorbed at $x = 1$. We notice that particles are allowed to explore the whole domain $[-\infty, 1]$. As it is customary, the translocation time in our simulations is the time of first arrival at the absorbing boundary $t_{\rm Tr} = \min\{t \in [0, T_w] : x(t) = 1\}$.

Figure 4 illustrates the average translocation time τ over the M trajectories as a function of the external load F (cf. Section III). The points are the results of the Brownian dynamic simulations and for comparison, the analytical curve Eq. (9) is also plotted, demonstrating the agreement with the numerical data. Different regimes are apparent in the behavior of $\tau(F)$. For high forcing, the typical inverse Gaussian behavior, $\tau = F^{-1}$, is recovered (lower horizontal dashed line). The stability threshold F_c for the onset of this ballistic-like regime can be roughly estimated as $F_c = \max_x \bar{U}'(x) \simeq 64.5$, that is, the minimal F-value after which the barrier of the tilted profile $G(x) = \bar{U}(x) - Fx$ disappears.[38–40] Below F_c, τ abruptly increases as the barrier crossing turns to be mainly thermally activated. The vertical line in Fig. 4 represents the threshold F_c separating a thermally activated from a ballistic-like regime.

TABLE I. Multi-Gaussian fit coefficients, Eq. (20), with a 95% confidence intervals. $\bar{U}_k$ are in k_BTe^{-1} while x_k and c_k are in Å.

k	$\bar{U}_k$	x_k	c_k
0	−0.547	−50.000	20.260
1	−4.000	1.000	29.230
2	2.510	18.940	11.110
3	0.729	49.243	0.003
4	1.047	50.432	4.396
5	8.340	52.766	35.590
6	1.112	68.610	125.000
7	0.598	92.130	7.732

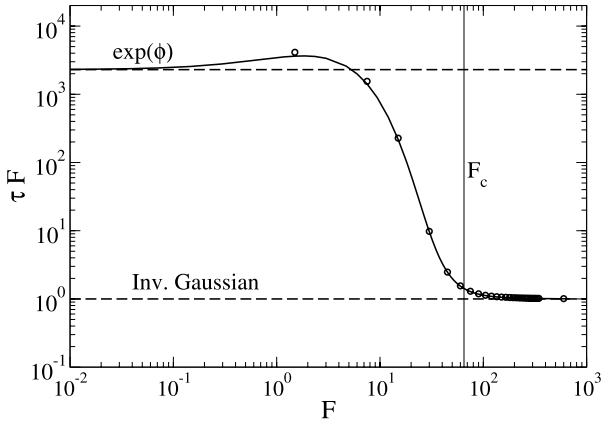

FIG. 4. Behavior of the average translocation time τ versus F. The solid line is the analytic result Eq. (9) while the points refer to numerical simulations. For high forcing ($F > F_c$), the curve collapses on the ballistic (inverse Gaussian) prediction $\tau = 1/F$. The higher dashed line indicates the $F = 0$ limit, Eq. (18). The vertical line marks the stability threshold $F_c = \max_x U'(x)$ at which the profile $G(x) = \bar{U}(x) - F_c x$ loses its stable minimum given by the solution $U'(x) = F$.

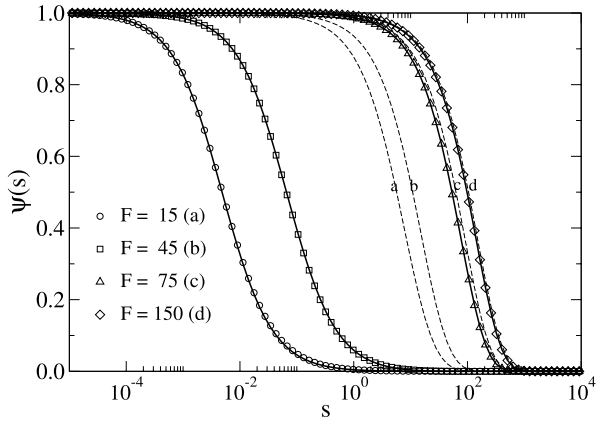

FIG. 5. Empirical Laplace transform for electrostatic barrier data, at $F = 15$ (circle), $F = 45$ (squares), $F = 75$ (triangle), $F = 150$ (diamonds). The solid lines are the Laplace transforms of $\hat{\psi}(s)$ for the square barrier. For each F, the equivalent barrier height ϕ is estimated by formula (23): $\phi(15) \simeq 8.13$, $\phi(45) \simeq 4.21$, $\phi(75) \simeq 3.14$, and $\phi(150) \simeq 2.365$. The dashed curves labelled by a–d indicate the Laplace transform of the inverse Gaussian computed at fields $F = 15, 45, 75, 150$, respectively. Clearly, the inverse Gaussian becomes a reasonable approximations only for high enough force.

Moreover, it is apparent that for low forcing the exit-time goes as Eq. (18).

Further analysis on translocation statistics can be carried out by collecting histograms of the first exit time from the $x = 1$ boundary. Since no analytical expressions are available for the $\psi(t)$ in the presence of the generic potential, we need to resort to the equivalent square-barrier approximation that, however, provides explicit formulas only in Laplace transform space. Therefore, a direct comparison of the normalized histograms with approximated results (13) requires the Laplace-inversion $\psi(t) = \mathcal{L}^{-1}[\psi(s)]_t$, which should be numerically performed via standard algorithm. To avoid the iteration of a boring fitting procedure made of a step of numerical inversion followed by a step of parameter tuning in Eq. (13), it is convenient to employ the so called *empirical* Laplace transform[29] which for a set of M measured exit times $\{t_k\}_{k=1}^{M}$ is defined as

$$\psi_e(s) = \frac{1}{M} \sum_{k=1}^{M} e^{-st_k}. \tag{22}$$

In this way, instead of comparing the distributions, we compare their Laplace transform; in other words, the comparison between data and theory is not done in the time-argument, as natural, but in the s-argument. In Fig. 5, the symbols represent the $\psi_e(s)$ associated to four sets of exit times at different values of F. The solid lines correspond to Eq. (13) with the barrier height ϕ estimated by inverting Eq. (17),

$$\phi = \ln\left\{1 + \frac{F(F\tau - 1)}{1 - e^{-F}}\right\}, \tag{23}$$

where τ is the numerical value obtained from formula (9). The agreement between $\psi_e(s)$ and Eq. (13) is striking and indicates that the shape of the time distribution can be well captured by adjusting a step-like barrier, regardless of the details of the true potential. The dashed lines from the left to the right refer to the inverse Gaussian computed at fields $F = 15, 45, 75, 150$, respectively. We see that at low and moderate fields $F = 15, 45$, the inverse Gaussian yields a bad representation of the exit time process. This comparison between data and theory via the Laplace transform suggests that even the simplest correction to the inverse Gaussian model is just able to drastically improve the description of the translocation time distribution in the regimes of small fields where the inverse Gaussian is known to be not applicable. To confirm the above scenario, we numerically inverted Eq. (13) via the fixed Talbot algorithm[41] implemented in Mathematica Wolfram 8.0 by Abate and Valkó[42] (package FixedTalbotNumericalLaplaceInversion.m) using the equivalent ϕ from Eq. (23).

The distributions of t for three different forcings are reported in Fig. 6 where the normalized histograms are represented by the shaded areas, whereas the solid curve indicates the theoretical distribution from the equivalent square barrier model. The first panel refers to the very low forcing regime ($F \ll F_c$) where the distribution is basically dominated by the exponential tail. At low forcing, $F < F_c$, the distribution of panel (b) is strongly skewed and develops a long tail for large t that yet differs from the inverse Gaussian as the waiting time before the barrier jumps cannot be neglected. Finally, panel (c) illustrates a case with $F > F_c$, and $\psi(t)$ does not differ qualitatively from the corresponding inverse Gaussian with the same value of F; at strong fields indeed, the barrier height is drastically reduced and the jump process becomes irrelevant. The insets of Fig. 6 report the lin-log plot of the main panel data, showing the good agreement between histograms and theoretical PdF also in the long-time tails. Moreover, the dashed straight lines represent the exponential decay of the tails as predicted by formula (16) and derived in Appendix B. The perfect alignment of the dashed line with the numerical inversion of Eq. (13) (solid line) in all the force regimes indicates that the behaviour predicted by Eq. (16) is an exact result. The agreement between theoretical predictions and simulation data is remarkable suggesting the general applicability of the square barrier model to obtain a first reasonable correction to the inverse Gaussian distribution.

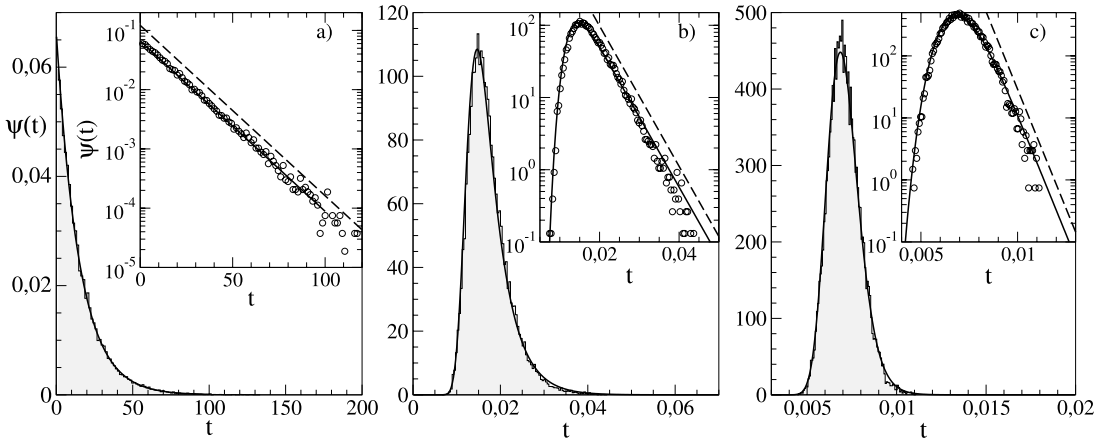

FIG. 6. Translocation time distributions over the electrostatic barrier, for three different external loads $F = 15$ (a), $F = 75$ (b), and $F = 150$ (c). The shaded areas represent the histograms collected from the arrival time at $L = 1$ of the trajectories generated by the numerical integration of Eq. (21). The black solid lines are the distribution computed with the model of equivalent-square barrier, with $\phi = 8.13$ (a), $\phi = 3.14$ (b), and $\phi = 2.365$ (c) set from Eq. (23); consider that no further parameter adjustment is required to fit perfectly the data. The insets are the lin-log plots of the main figures showing the exponential tail of the distributions predicted by Eq. (16) (dashed line).

V. CONCLUSIONS

Translocation of molecules through narrow nanopores is often described as one-dimensional driven diffusion over a energy or free-energy profile. This approach is justified as long as a single reaction coordinate is capable of characterizing the transport dynamics while the motion along any other direction can be considered to be much faster.[43] Although this assumption may not be true in general, one-dimensional models are considered useful mathematical tools to describe the qualitative features of the transport phenomenology across narrow pores.

In this paper, we investigated the diffusion of a single particle driven by an external constant field along a realistic energy profile. We worked out an analytical expression of the average translocation time for generic energy profiles, and of the Laplace transform of the translocation-time distribution over a square barrier. As a representative case to compare with our theoretical results, we selected the transport of a positive charged particle through an αHL pore, whose electrostatic potential has been computed via the *Poisson* equation.

In order to collect the statistics of the translocation time at different values of the forcing, we performed numerical simulations of the barrier crossing process by solving a Langevin equation. The average translocation time has been found to be in good agreement with the our analytical prediction. The energy landscape strongly affects the transport at low forcing, determining a non-trivial behavior of the average translocation time with the force intensity F. At high forcing, the role of the energy landscape can be neglected; thus, the translocation process is equivalent to a driven-diffusion mechanism without barriers. As a consequence, the average translocation time shows the quasi-ballistic F^{-1}-dependence.

Also, translocation time distributions clearly reflect the presence of these two forcing regimes. At low forcing, where the effects of the energy profile are particularly relevant, we were unable to derive the exact expression of such distributions, so we resorted to the simplest yet still meaningful approximation by replacing the actual potential barrier with an appropriate square profile. In this way, the true Laplace transform of the translocation-time distribution over the αHL electrostatic barrier is well approximated by the corresponding distribution in the model with the "*equivalent*" square barrier.

Working with the Laplace transform is convenient as it maps a differential equation problem into an algebraic one. However, the main difficulty relies in the inversion of the transformation, a step that is often done numerically. In this respect, we have shown that by employing *empirical Laplace transform* (22) of translocation-time raw data, the inversion procedure can be skipped, as the comparison between theoretical and numerical distributions is equivalent to comparing their respective transformations. We expect these observations to help the development of new methods based on empirical Laplace transforms for the analysis of experimental translocation data. Finally, we obtained the analytical decay law of the arrival-time distributions at large times for any square-barrier height and any explored forcing. This exponential behaviour $\psi_\phi(t) \sim \exp(-\gamma t)$ is controlled by the coefficient $\gamma = F^2 e^\phi/(1 + e^\phi)^2$ that depends both on the barrier height ϕ and the drive F.

APPENDIX A: DERIVATION OF ANALYTICAL EXPRESSION

In this appendix, we derive formulas (9) and (13) from the Smoluchowski equation for a particle in a potential $G(x) = \bar{U}(x) - Fx$, where $\bar{U}(x)$ is significantly non-zero only in the region $[0, 1]$, Fig. 3 while F acts over $]-\infty, 1]$. We use natural variables to get a dimensionless equation and we consider the Laplace transform

$$Y(x,s) = \int_0^\infty dt P(x,t) e^{-st} \tag{A1}$$

of the probability distribution, which satisfies the equation

$$sY(x,s) - \delta(x) = \frac{\partial}{\partial x}\left\{\frac{\partial Y(x,s)}{\partial x} + G'(x)Y(x,s)\right\} \tag{A2}$$

with initial condition $P(x,0) = \delta(x)$. This problem cannot be solved in a closed form except for some special choice of

$G(x)$; yet, according to (8), the exact expression of the average translocation time derives from the solution of the simplified problem with $s = 0$,

$$\tau = \int_{-\infty}^{1} dx Y(x,0). \tag{A3}$$

As it is customary, the presence of the term $\delta(x)$ in (A2) requires to solve the homogeneous equation

$$\frac{\partial}{\partial x}\left\{\frac{\partial Y(x,0)}{\partial x} + G'(x)Y(x,0)\right\} = 0 \tag{A4}$$

in each of the two domains $R_1 =]-\infty, 0[$ and $R_2 = [0,1]$,

$$Y(x) = \begin{cases} a_0 e^{Fx} & \text{if } x < 0 \\ e^{-G(x)}[a_1 + b_1 \int_0^x d\xi e^{G(\xi)}] & \text{if } 0 \le x \le 1 \end{cases},$$

where we omit writing $s = 0$ for simplicity. The coefficients are determined by the boundary conditions $Y(-\infty) = Y(1) = 0$ and by the two matching conditions at $x = 0$, resulting from the continuity, $Y(0^+) = Y(0^-)$, and from integrating both members of Eq. (A4) over the interval $[-\epsilon, \epsilon]$ then taking $\epsilon \to 0$ (see Ref. 44, pp. 112-116). The latter leads to the following current jump:

$$\begin{aligned} -1 = &[Y'(x) + G'(x)Y(x)]_{x=0^+} \\ &- [Y'(x) + G'(x)Y(x)]_{x=0^-} \end{aligned} \tag{A5}$$

which, assuming the continuity of $\bar{U}'(x)$ and $Y(x)$ in $x = 0$, reduces to $-1 = Y'(0^+) - Y'(0^-)$. In other words, the derivative $\partial_x Y$ presents a discontinuity of magnitude 1 in $x = 0$. These three conditions determine univocally the coefficients a_0, a_1, b_1, which read

$$a_0 = -a_1 = \int_0^1 dq e^{\bar{U}(q) - Fq}, \qquad b_1 = -1.$$

Then, according to formula (A3), the direct integration of $Y(x)$ over $]-\infty, 1]$ yields result (9),

$$\tau = \frac{a_0}{F} + \int_0^1 dx e^{\bar{U}(x) - Fx} \int_x^1 dy e^{-\bar{U}(y) + Fy}.$$

The case with a square barrier in $[0,1]$, $\bar{U}(x) = \phi\Theta[x(1-x)]$, $\Theta(s)$ being the unitary step function, has the advantage of being fully tractable even for $s \neq 0$. In this case, Eq. (A2) reduces to

$$Y''(x,s) - FY'(x,s) - sY(x,s) = 0, \tag{A6}$$

whose solutions in R_1 and R_2 are linear combinations of $\exp(Fx/2 \pm \sqrt{F^2 + 4s}/2)$, i.e.,

$$Y(x,s) = \begin{cases} e^{Fx/2}(A_1 e^{qx} + A_2 e^{-qx}) & x < 0 \\ e^{Fx/2}(B_1 e^{qx} + B_2 e^{-qx}) & 0 \le x \le 1 \end{cases}, \tag{A7}$$

with $q = \sqrt{F^2 + 4s}/2$. As before, the four coefficients A_1, A_2, B_1, B_2 are determined by the boundary conditions: $Y(-\infty, s) = 0$, $Y(1,s) = 0$ and by the matching at the discontinuity of the potential, $Y(0^+, s)e^{\phi} = Y(0^-, s)$, in which the barrier height ϕ appears.[45] Again, the presence of the δ-function imposes constraint (A5),

$$-1 = Y'(0^+, s) - FY(0^+, s) - [Y'(0^-, s) - FY(0^-, s)].$$

After simple but tedious algebra, we obtain the following solution:

$$Y(x,s) = \begin{cases} h_1(s)\, e^{Fx/2} \exp(qx) & x < 0 \\ h_2(s)\, e^{Fx/2} \sinh[q(1-x)] & 0 \le x \le 1 \end{cases}, \tag{A8}$$

where the coefficients h_1, h_2 read

$$\begin{aligned} h_1(s) &= \frac{2e^{\phi}\sinh(q)}{2q\cosh(q) + [2e^{\phi}q - F(e^{\phi} - 1)]\sinh(q)}, \\ h_2(s) &= \frac{2}{2q\cosh(q) + [2e^{\phi}q - F(e^{\phi} - 1)]\sinh(q)}. \end{aligned} \tag{A9}$$

Thus, after Laplace transforming Eq. (7), which yields $\hat{\psi}(s) = J(1,s)$, we have

$$\hat{\psi}_{\phi}(s) = \frac{e^{F/2}\sqrt{F^2 + 4s}}{\sqrt{F^2 + 4s}\cosh\left(\frac{1}{2}\sqrt{F^2 + 4s}\right) + \left[e^{\phi}\sqrt{F^2 + 4s} - F(e^{\phi} - 1)\right]\sinh\left(\frac{1}{2}\sqrt{F^2 + 4s}\right)}, \tag{A10}$$

that is, Equation (13) reported in Section III. When $\phi = 0$, we simply recover the Laplace transform of inverse Gaussian (14),

$$\hat{\psi}_{\phi}(s) = e^{\frac{1}{2}\left(F - \sqrt{F^2 + 4s}\right)}. \tag{A11}$$

APPENDIX B: LAPLACE INVERSION

For the sake of completeness we report additional explicit calculations concerning the inversion of the Laplace transform. Using the shift property of the Laplace transformation, such that $s \to s - F^2/4$, Eq. (A10) can be recast into the following form:

$$\psi_{\phi}(t) = \exp\left\{-\frac{F^2 t}{4} + \frac{F}{2}\right\}\mathcal{L}^{-1}[\hat{Q}(\sqrt{s})]_t, \tag{B1}$$

hereafter, $\mathcal{L}^{-1}[\ldots]_u$ indicates the inverse Laplace transform of argument u. Thus, we are left with the simpler function to be inverted

$$\hat{Q}(\sqrt{s}) = \frac{2\sqrt{s}}{2\sqrt{s}\cosh(\sqrt{s}) + \left[2e^{\phi}\sqrt{s} - F(e^{\phi} - 1)\right]\sinh(\sqrt{s})}, \tag{B2}$$

that can be recast in the form

$$\hat{Q}(\sqrt{s}) = \frac{2\sqrt{s}}{e^{\sqrt{s}}[(e^{\phi} + 1)\sqrt{s} - w] - e^{-\sqrt{s}}[(e^{\phi} - 1)\sqrt{s} - w]},$$

where $w = F(e^{\phi} - 1)/2$. In order to use Laplace transform tables of elementary functions, $\hat{Q}(\sqrt{s})$ can be conveniently rewritten as a geometric series

$$\hat{Q}(\sqrt{s}) = \frac{2\sqrt{s}\, e^{-\sqrt{s}}}{a\sqrt{s} - w} \sum_{n=0}^{\infty} e^{-2n\sqrt{s}} \left(1 - \frac{2\sqrt{s}}{a\sqrt{s} - w}\right)^n, \quad \text{(B3)}$$

with $a = e^{\phi} + 1$.

It is immediate to treat the case $F = 0 (w = 0)$, i.e., barrier without drift, that reduces to invert

$$\hat{Q}(\sqrt{s}) = \frac{2}{a} \sum_{n=0}^{\infty} e^{-(2n+1)\sqrt{s}} \left(1 - \frac{2}{a}\right)^n \quad \text{(B4)}$$

leading to the formula

$$\psi_{\phi}^{(0)}(t) = \frac{2}{1 + e^{\phi}} \sum_{n=0}^{\infty} \left(\frac{e^{\phi} - 1}{e^{\phi} + 1}\right)^n \frac{2n+1}{\sqrt{4\pi t^3}} \exp\left\{-\frac{(2n+1)^2}{4t}\right\}. \quad \text{(B5)}$$

When t is large, sum (B5) is dominated by the $n = 0$ term; thus, we obtain the asymptotic approximation

$$\psi_{\phi}^{(0)}(t) \simeq \frac{2}{1 + e^{\phi}} \frac{\exp\{-1/(4t)\}}{\sqrt{4\pi t^3}}.$$

For the case $F > 0$, we perform a further binomial expansion of the term raised to the n-power in Eq. (B3),

$$\hat{Q}(\sqrt{s}) = \sum_{n=0}^{\infty} \sum_{k=0}^{n} (-1)^k \binom{n}{k} \left(\frac{2\sqrt{s}}{a\sqrt{s} - w}\right)^{k+1} e^{-t_n\sqrt{s}} \quad \text{(B6)}$$

and for shortness sake, we set $t_n = 2n + 1$ and

$$\hat{Q}_{n,k}(\sqrt{s}) = \left(\frac{2\sqrt{s}}{a\sqrt{s} - w}\right)^{k+1} e^{-t_n\sqrt{s}}.$$

Applying the Schouten-Van der Pol theorem (see Ref. 46 and p. 77 of Ref. 47) we can invert each term of sum (B6) with $\sqrt{s}$ replaced by s at the price of solving the integral

$$\mathcal{L}^{-1}[\hat{Q}_{n,k}(\sqrt{s})]_t = \int_0^{\infty} \frac{du\, u}{\sqrt{4\pi t^3}} e^{-u^2/4t}\, \mathcal{L}^{-1}[\hat{Q}_{n,k}(s)]_u. \quad \text{(B7)}$$

It can be shown that

$$\mathcal{L}^{-1}[\hat{Q}_{n,k}(s)]_u = \left(\frac{2}{a}\right)^{k+1} \left[\delta(u - t_n) + (k+1)\frac{w}{a}\Theta(u - t_n) M\left(k+2, 2, \frac{w(u - t_n)}{a}\right)\right], \quad \text{(B8)}$$

where $\Theta(u - t_n)$ is the unitary step function and $M(\alpha, \beta, u)$ indicates the Kummer's confluent hypergeometric function[48] which for $\alpha = k + 2$ and $\beta = 2$ is known to assume the form $M(k+2, 2, x) = e^x P_k(x)$ of a product between an exponential and a polynomial of degree k, such that $P_0(x) = P_k(0) = 1$.

The above expression plugged into the integral (B7) yields

$$\mathcal{L}^{-1}\left[\hat{Q}_{n,k}(\sqrt{s})\right]_t = \left(\frac{2}{a}\right)^{k+1} \left[\frac{t_n\, e^{-t_n^2/(4t)}}{\sqrt{4\pi t^3}} + (k+1)\frac{w}{a} I_{n,k}(t)\right], \quad \text{(B9)}$$

where $I_{p,q}(t)$ represents the integral

$$I_{p,q}(t) = \int_0^{\infty} \frac{du(u + t_p)}{\sqrt{4\pi t^3}} \exp\left\{-\frac{(u + t_p)^2}{4t} + \frac{wu}{a}\right\} P_q\left(\frac{wu}{a}\right).$$

Combining all the above expressions together and considering that the first term of Eq. (B9) reconstructs function Eq. (B5), we obtain the final result as a sum

$$\mathcal{L}^{-1}\left[\hat{Q}(\sqrt{s})\right] = \psi_n^{(0)}(t) + \frac{w}{a} \sum_{(n,k)=0}^{\infty} g(n+k, k) I_{n+k,k}(t) \quad \text{(B10)}$$

with coefficients

$$g(p, q) = (-1)^q \binom{p}{q} \left(\frac{2}{a}\right)^{q+1} (q + 1).$$

The substitution of Eq. (B10) into Eq. (A10) yields the first arrival time distribution, which, despite the simplicity of the problem, remains quite involved as it amounts to a double series in the k, n indexes. However, one can easily derive the simplest nontrivial correction to Eq. (B5) ($F = 0$ case) by retaining only the $k = 0$ terms in Eq. (B10),

$$\psi_{\phi}(t) \simeq e^{-F^2 t/4 + F/2} \left[\psi_{\phi}^{(0)}(t) + F\frac{e^{\phi} - 1}{(e^{\phi} + 1)^2} \sum_{n=0}^{\infty} I_{n,0}(t)\right]. \quad \text{(B11)}$$

As a final remark, we stress that asymptotic behaviour of $\psi_{\phi}(t)$ at large times is fully determined, term by term, by the explicit structure of the integrals $I_{p,q}(t)$. The large-t behaviour of $I_{p,q}(t)$ can be estimated by evaluating the integrand at the saddle point $u^* = 2tw/a - t_p$ of its exponent. The direct substitution shows that $I_{p,q}(t) \sim \exp[t(w/a)^2]$ which combined with the exponent $-F^2 t/4$ from Eq. (B1), and recalling that $\psi_{\phi}^{(0)}(t) \sim t^{-3/2}$ is subleading, yields the large-time behaviour of the distribution

$$\psi_{\phi}(t) \sim \exp\left\{-\frac{e^{\phi} F^2}{(e^{\phi} + 1)^2} t\right\}. \quad \text{(B12)}$$

where, we substituted $w = F/2(e^{\phi} - 1), a = e^{\phi} + 1$. The analytical result, Eq. (B12), is an exact asymptotic property of the arrival-time distribution of the driven-diffusion over a square barrier, as it verified with great accuracy in the explored range of F by the numerical inversion of Eq. (13) in Fig. 6.

[1] S. Matysiak, A. Montesi, M. Pasquali, A. B. Kolomeisky, and C. Clementi, Phys. Rev. Lett. **96**, 118103 (2006).
[2] C.-T. A. Wong and M. Muthukumar, J. Chem. Phys. **128**, 154903 (2008).
[3] L. Huang and D. Makarov, J. Chem. Phys. **129**, 121107 (2008).
[4] M. Chinappi, F. Cecconi, and C. M. Casciola, Philos. Mag. **91**, 2034 (2011).
[5] M. Bacci, M. Chinappi, C. M. Casciola, and F. Cecconi, J. Phys. Chem. B **116**, 4255 (2012).
[6] A. M. Berezhkovskii, M. A. Pustovoit, and S. M. Bezrukov, J. Chem. Phys. **116**, 9952 (2002).

[7]M. Muthukumar, *Polymer Translocation* (Taylor & Francis US, 2011).
[8]L. Movileanu, J. P. Schmittschmitt, J. M. Scholtz, and H. Bayley, Biophys. J. **89**, 1030 (2005).
[9]C.-T. A. Wong and M. Muthukumar, J. Chem. Phys. **133**, 045101 (2010).
[10]M. Muthukumar and C. Y. Kong, Proc. Natl. Acad. Sci. U. S. A. **103**, 5273 (2006).
[11]D. Panja, G. T. Barkema, and A. B. Kolomeisky, J. Phys.: Condens. Matter **25**, 413101 (2013).
[12]J. L. Trick, E. J. Wallace, H. Bayley, and M. S. Sansom, ACS Nano **8**, 11268 (2014).
[13]L. Mereuta, M. Roy, A. Asandei, J. K. Lee, Y. Park, I. Andricioaei, and T. Luchian, Sci. Rep. **4**, 3885 (2014).
[14]D. K. Lubensky and D. R. Nelson, Biophys. J. **77**, 1824 (1999).
[15]A. Ammenti, F. Cecconi, U. Marini Bettolo Marconi, and A. Vulpiani, J. Phys. Chem. B **113**, 10348 (2009).
[16]A. Pelizzola and M. Zamparo, Europhys. Lett. **102**, 10001 (2013).
[17]W. Im and B. Roux, J. Mol. Biol. **322**, 851 (2002).
[18]M. Bacci, M. Chinappi, C. M. Casciola, and F. Cecconi, Phys. Rev. E **88**, 022712 (2013).
[19]C. W. Gardiner, Springer Ser. Synergetics **13**, 2963–2968 (1985).
[20]L. Song, M. R. Hobaugh, C. Shustak, S. Cheley, H. Bayley, J. E. Gouaux *et al.*, Science **274**, 1859 (1996).
[21]C. Madampage, O. Tavassoly, C. Christensen, M. Kumari, and J. Lee, Prion **6**, 110 (2012).
[22]A. G. Oukhaled, A. L. Biance, J. Pelta, L. Auvray, and L. Bacri, Phys. Rev. Lett. **108**, 88104 (2012).
[23]A. G. Oukhaled, J. Mathe, A. Biance, L. Bacri, J. Betton, D. Lairez, J. Pelta, and L. Auvray, Phys. Rev. Lett. **98**, 158101 (2007).
[24]J. Nivala, D. B. Marks, and M. Akeson, Nat. Biotechnol. **31**, 247 (2013).
[25]D. Rodriguez-Larrea and H. Bayley, Nat. Nanotechnol. **8**, 288 (2013).
[26]A. Asandei, M. Chinappi, J.-k. Lee, C. H. Seo, L. Mereuta, Y. Park, and T. Luchian, Sci. Rep. **5**, 10419 (2015).
[27]D. Di Marino, E. L. Bonome, A. Tramontano, and M. Chinappi, J. Phys. Chem. Lett. **6**, 2963–2968 (2015).
[28]A. Asandei, M. Chinappi, H.-K. Kang, C. H. Seo, L. Mereuta, Y. Park, and T. Luchian, ACS Appl. Mater. Interfaces **7**, 16706–16714 (2015).
[29]N. Henze and B. Klar, Ann. Inst. Stat. Math. **54**, 425 (2002).
[30]T. J. Dolinsky, P. Czodrowski, H. Li, J. E. Nielsen, J. H. Jensen, G. Klebe, and N. A. Baker, Nucleic Acids Res. **35**, W522 (2007).
[31]J. Wang, P. Cieplak, and P. A. Kollman, J. Comput. Chem. **21**, 1049 (2000).
[32]M. Holst, Adv. Comput. Math. **15**, 139 (2001).
[33]A. Manzin, D. Ansalone, and O. Bottauscio, IEEE Trans. Magn. **47**, 1382 (2011).
[34]A. Manzin, O. Bottauscio, and D. Ansalone, J. Comput. Chem. **32**, 3105 (2011).
[35]N. A. Simakov and M. G. Kurnikova, J. Phys. Chem. B **114**, 15180 (2010).
[36]D. Y. Ling and X. S. Ling, J. Phys.: Condens. Matter **25**, 375102 (2013).
[37]R. L. Honeycutt, Phys. Rev. A **45**, 600 (1992).
[38]O. K. Dudko, G. Hummer, and A. Szabo, Phys. Rev. Lett. **96**, 108101 (2006).
[39]M. Evstigneev and P. Reimann, J. Phys.: Condens. Matter **27**, 125004 (2015).
[40]C. A. Plata, F. Cecconi, M. Chinappi, and A. Prados, J. Stat. Mech.: Theory Exp. **2015**, P08003.
[41]A. Talbot, IMA J. Appl. Math. **23**, 97 (1979).
[42]J. Abate and P. Valkó, Int. J. Numer. Methods Eng. **60**, 979 (2004).
[43]A. Berezhkovskii and A. Szabo, J. Chem. Phys. **135**, 074108 (2011).
[44]H. Risken, *The Fokker-Planck Equation: Methods of Solution and Applications*, Lecture Notes in Mathematics (Springer, 1996).
[45]V. Berdichevsky and M. Gitterman, J. Phys. A: Math. Gen. **29**, 1567 (1996).
[46]J. Schouten, Physica **2**, 75 (1935).
[47]D. Duffy, *Transform Methods for Solving Partial Differential Equations*, 2nd ed. (CRC Press, 2004), p. 77.
[48]G. B. Arfken and H. J. Weber, *Mathematical Methods For Physicists*, International Student Edition (Academic Press, 2005).